

Aminoglycoside Association Pathways with the 30S Ribosomal Subunit

Maciej Dlugosz* and Joanna Trylska

Interdisciplinary Centre for Mathematical and Computational Modelling, University of Warsaw,
Pawińskiego 5A, 02-106 Warsaw, Poland

Received: December 21, 2008; Revised Manuscript Received: March 4, 2009

Many aminoglycoside antibiotics target bacterial ribosomes and alter their proper functioning as translational machinery leading to bacterial death. To better understand their several inhibitory mechanisms we applied Brownian dynamics and investigated the kinetics and association of paromomycin, an aminoglycoside representative, with the entire 30S ribosomal subunit. We determined that aminoglycoside specific binding at the ribosomal aminoacyl-tRNA site (A-site) begins with antibiotic diffusion toward any point on the 30S subunit and is followed by exploration of the 30S surface. Surprisingly, there is no direct electrostatic steering of the antibiotic to the A-site. Furthermore, we discovered two possible entrances to the A-site around which the mobility of paromomycin is high. The antibiotic also visits binding sites for other drugs targeting the 30S subunit. We found that paromomycin interacts with different sites located along the helix 44 of 16S rRNA, which might explain the recent experimental findings that paromomycin's other inhibitory role arises from overstabilizing the ribosomal 70S complex. In addition, our simulations revealed an alternate binding cleft in the 30S subunit that may be important for paromomycin's inhibitory effect on translocation. The diffusion limited rate of association was estimated of the order of $10^9 \text{ (M}\cdot\text{s})^{-1}$ with no dependence on the ionic strength of the solution; the physical origins of this result are explained.

Introduction

Proteins are synthesized on the ribosome whose role is to translate the genetic information stored in the mRNA into a specific amino acid sequence. The ribosome itself is a massive macromolecular complex composed in bacteria of three RNA chains and over 50 proteins. It consists of two subunits, named according to their sedimentation coefficients, 50S (large) and 30S (small), which associate through a network of intersubunit bridges to form a 70S ribosome. The 30S subunit is composed of ~1500 nucleotide long 16S rRNA and 21 proteins that are labeled S1, S2,... etc. There are three tRNA binding sites on the ribosome. The cognate aminoacyl-tRNA binds at the A-site located at the top of ribosomal helix 44 in the 30S subunit (Figure 1). The A-site is also a target for various antibiotics among them paromomycin that belongs to the aminoglycoside family. Paromomycin consists of four pseudosugar rings with amino and hydroxyl substituents and at physiological pH carries a positive total charge of +5e.¹

The antibacterial role of aminoglycosides has been known for at least six decades. However, their use in medical therapy is significantly impeded by their moderate affinity and inadequate specificity. Aminoglycosides have been associated with causing damages to ear and kidney cells. Therefore, further studies are needed to elucidate their inhibitory role on bacterial translation.

The binding of aminoglycosides at the ribosomal A-site decreases the fidelity of translation. As a result, defective polypeptide chains are synthesized that eventually leads to bacterial death. Crystal structures of paromomycin complexed with 30S subunits^{2,3} show that upon antibiotic binding at the A-site two nucleotides, numbered in *E. coli* A1492 and A1493, bulge outward from their original base-stacked position inside

helix 44 (Figure 2). Paromomycin's antibacterial action arises from its ability to stabilize A1492 and A1493 in a flipped-out state locking the A-site in a conformation in which discrimination of cognate and near-cognate tRNAs is diminished.^{4–6}

However, it was also shown that paromomycin inhibits the assembly of the 30S ribosomal subunit and promotes the accumulation of the 21S intermediate particle.^{7,8} The inhibitory effect on the 30S formation is approximately equivalent to the inhibitory effect on the translation itself but a detailed mechanism is not known. Four proteins—S2, S3, S10, S14—are not present in the natural 21S assembly intermediate.⁹ These proteins, interacting with the 3' domain of 16S RNA, are classified as late (according to kinetic footprinting experiments)¹⁰ or tertiary (according to 30S assembly order mapping)^{11,12} binding proteins. Another recently discovered inhibitory effect shows that paromomycin (similar to Mg²⁺ ions and polyamines) strengthens the interaction between 30S and 50S subunits. This stabilizes the 70S complex also affecting its internal mobility needed for translocation of tRNAs and precludes timely dissociation of subunits after the termination of protein synthesis.¹³ In the latter case the mechanism of inhibition is also not fully clarified.

In recent years, crystal and NMR structures of several aminoglycosides bound to the A-site RNA constructs,^{14–17} as well as to the entire 30S subunit^{2,3,18,19} were solved. This resulted in a number of computational studies that described the structural properties and energetics of RNA/aminoglycoside complexes and the behavior of aminoglycoside binding to different RNA motifs or A-site RNA fragments.^{20–24} Theoretical studies involving the entire 30S subunit complexed with aminoglycosides are mostly limited to energetic aspects.^{25,26} Therefore, the focus of work was to investigate both aminoglycoside association pathways and kinetics of binding to the 30S subunit.

We applied Brownian dynamics (BD) which is a mesoscale simulation method commonly used to study solute–solvent

* To whom correspondence should be addressed. E-mail: mdlugosz@icm.edu.pl

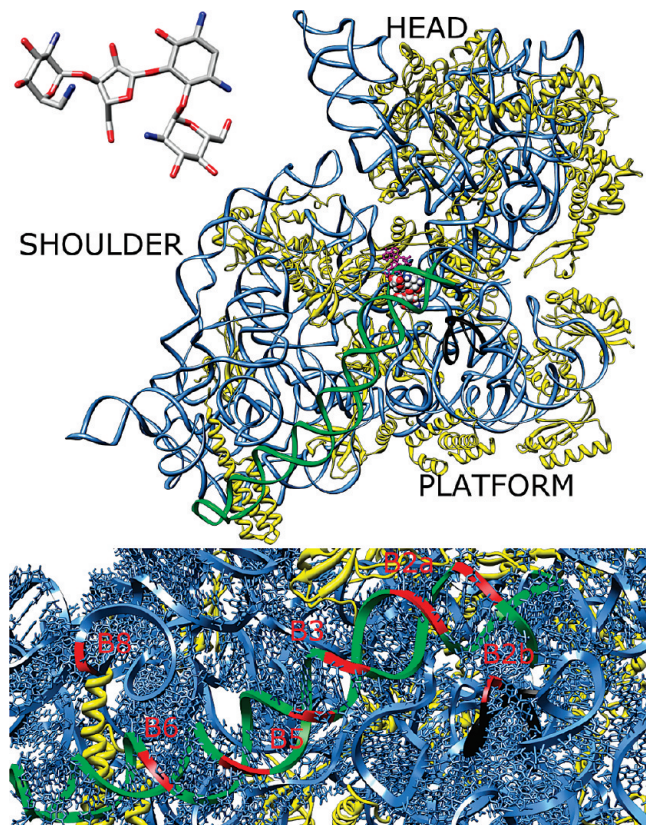


Figure 1. The structure of the 30S ribosomal subunit from *Thermus thermophilus* complexed with paromomycin (PDB code 1IBK). (Top) View of the interface side between the two ribosomal subunits, that is, the 50S-exposed side. Proteins are shown in yellow, 16S RNA in blue, helix 44 in green, helix 45 in black, and A1492 and A1493 as magenta sticks. Paromomycin (van der Waals spheres) is colored according to atom types and its heavy-atom stick model is shown in the top left corner. (Bottom) Zoom of the interface between the two subunits with intersubunit bridges indicated in red.

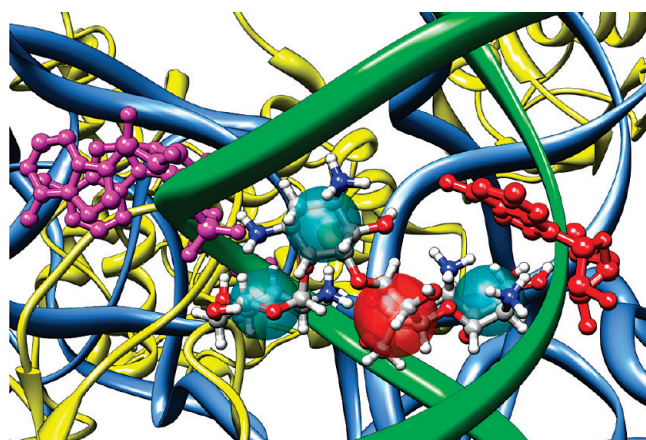


Figure 2. Zoom of the A-site with ball and stick and bead models (partially transparent spheres) of paromomycin. During BD, the distance between the backbone phosphorus atom of G1405 (in red) and the central red bead of paromomycin was monitored as the reaction criterion. Helix 44 is shown in green, and A1492 and A1493 are in magenta.

systems without explicitly considering the solvent particles. BD has proven to be particularly useful in the studies of the diffusional motion between interacting solutes. Its applications to protein–protein,^{27,28} protein–ligand,²⁹ and DNA/RNA-ligand^{24,30} systems provide estimations of diffusion limited rates of association and give insight into mechanisms of formation

of molecular complexes. We used BD to study the association mechanism of paromomycin with the 30S subunit (Figure 1), estimate the association rates, examine their dependence on the ionic strength of the solution, and describe the behavior of the antibiotic near the surface of the 30S subunit. The 30S subunit is composed of about 95000 atoms and paromomycin of only 92 atoms. The solvent accessible surface area of the 30S subunit is roughly $2.5 \times 10^5 \text{ \AA}^2$ and that of paromomycin about $8.1 \times 10^2 \text{ \AA}^2$. This 3 orders of magnitude difference in scales and high density of negative charges accumulated on the 16S rRNA phosphate groups poses a great challenge from the computational standpoint not only regarding the computer time and resources but also data analysis.

We investigate how such a small antibiotic can find its binding site on the 30S subunit. What is the role of electrostatic interactions in this association? Considering the distribution and density of negative charges on the surface of the 30S subunit, is there a dominant electrostatic steering straightforwardly directing the positively charged antibiotic to the A-site? Are electrostatic interactions solely responsible for discrimination between different fragments of rRNA by the antibiotic? Can the association pathways explain other paromomycin inhibitory roles? We believe that some of these questions cannot be fully answered while studying only the isolated A-site RNA constructs and the studies of antibiotic binding to the entire 30S subunit are necessary and, therefore, conducted in this work.

Theory and Methods

Structures. Coordinates of the *Thermus thermophilus* 30S ribosomal subunit complexed with paromomycin (Figure 1), determined at 3.3 Å resolution, were taken from the PDB³¹ (1IBK entry).³ Atomic charges and radii were assigned according to AMBER 8³² force field with standard protonation states of titratable amino acids. Two structures were prepared: the whole 30S subunit with a total charge (including crystal Mg²⁺ and Zn²⁺ ions) of $-1032e$, and its variant lacking S2, S3, S10, and S14 proteins with a total charge of $-1066e$. It was shown³³ that tertiary binding proteins are less important for stabilizing the 16S RNA three-dimensional structure than the early binders; thus, we simply removed the four appropriate chains from the PDB file and did not alter the remaining parts of the 30S subunit. Paromomycin partial charges were determined with the bcc option of ANTECHAMBER.³⁴ Because paromomycin was proven to be fully protonated upon binding to the ribosomal A-site,¹ all its amino groups were kept protonated to give a total charge of $+5e$. The positions of added hydrogens were energy-minimized using the SANDER module of AMBER 8³² and the steepest descent method.

Brownian dynamics. Two Brownian particles, a fixed acceptor and a ligand, are placed in their initial configurations (Figure 3). The ligand, composed of spherical subunits and subjected to both external and intersubunit forces, is moved along the trajectory following the Ermak–McCammon propagation scheme:³⁵

$$\mathbf{r}_i^{n+1} = \mathbf{r}_i^n + \sum_j \frac{\Delta t}{k_B T} D_{ij} F_j^n + R_i(\Delta t) \quad (1)$$

where indices i and j run over the coordinates of N subunits ($i, j \leq 3N$), r_i is the position vector component, F_j is the sum of intersubunit and external forces acting in direction j , integer n denotes discrete times $t = n\Delta t$ at intervals Δt , and D_{ij} is a configuration dependent diffusion tensor (with the diffusion coefficient of the acceptor summed into its diagonal parts). Each of the ligand's spherical subunits rotates and translates interact-

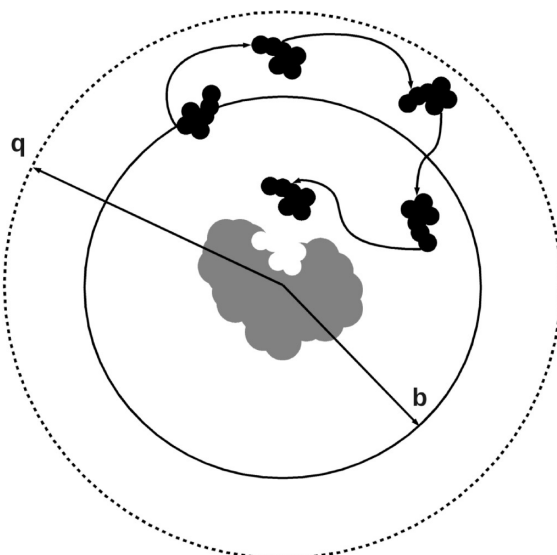


Figure 3. A diagram illustrating the BD method. The ligand (in black) diffuses relatively to a fixed acceptor (gray). The Ligand's starting positions and orientations are randomly chosen on the b sphere whose radius is assigned large enough to ensure that at distance b intermolecular forces are centrosymmetric. The trajectory is truncated if the ligand crosses the surface of the q sphere or if an encounter complex is formed.

ing hydrodynamically with others. The overall shape of the ligand is conserved by rigid bonds introduced between subunits that also ensure that the overall rotation and translation of the ligand follows its diffusional properties (in the sense of average diffusion coefficients). $R_i(\Delta t)$ is a random displacement with Gaussian distribution function fulfilling $\langle R_i \rangle = 0$ and $\langle R_i(\Delta t) R_j(\Delta t) \rangle = 2D_{ij}^n \Delta t$. In a BD simulation, only electrostatic contribution to intermolecular forces is taken into account, considering the ligand as a set of point charges centered on its spherical subunits. Steric interactions are modeled by preventing the overlap between a ligand's subunits and acceptor atoms. If after a given simulation step a steric clash is observed, the ligand is shifted back to its previous position and the simulation step is performed with a new random displacement vector. Other, short-range interactions, such as hydrogen bonding and van der Waals interactions, are neglected.

Calculation of Diffusional Bimolecular Rate Constants. BD trajectories are terminated either when a set of particular criteria of an encounter complex formation are met or when the separation of associating molecules becomes significant. A BD run is counted as successful when the encounter definitions are fulfilled. The rate of a reaction k is given by^{36,37}

$$k = \frac{k_D(b)\beta}{1 - (1 - \beta)\frac{k_D(b)}{k_D(q)}} \quad (2)$$

where β is determined as the ratio of successful BD runs to the total number of runs, and $k_D(x)_{x \in \{b,q\}}$ is the analytically computed rate in which the diffusing particles reach separation x (Figure 3).

Hydrodynamic Models of Paromomycin and 30S Subunit. First, the translational diffusion coefficient for all-atom structure of paromomycin was determined with HYDROPRO³⁸ as $3.2 \times 10^{-6} \text{ cm}^2 \text{ s}^{-1}$, using the procedure described in ref 24. Second, paromomycin rings were replaced with 4 beads (Figure 2). Beads were assigned hydrodynamic radii of 4.4 \AA using the software of J. Antosiewicz,³⁹ so that the diffusion coefficient of the bead model reproduced the value for the all-atom

structure. Beads were assigned a net charge in accord with the number of amino groups of a given ring. The overall shape of the antibiotic was maintained by the SHAKE algorithm⁴⁰ (with the 0.2 \AA tolerance) applied to four pseudobonds connecting the beads. Both variants of the 30S subunit were assigned the Stokes translational radius of 85 \AA .

Electrostatic Forces. Electrostatic interactions and forces were described with the Poisson–Boltzmann model⁴¹ that merges a microscopic model of a molecule with a mesoscopic description of solvent. A molecule is modeled as a set of spheres with centrally assigned partial charges that are immersed in a continuum, highly polarizable dielectric medium (with dielectric constant of water, $\epsilon \approx 80$) representing the solvent. Spheres form a dielectric body of low ϵ with a boundary defined for example, as molecular surface. Effects arising from dielectric heterogeneity and ionic strength are included through the Poisson–Boltzmann equation whose nonlinear form, appropriate for highly charged systems, is given with

$$\nabla \epsilon(\vec{r}) \nabla \psi(\vec{r}) + 4\pi \left[\rho(\vec{r}) + \sum_i e z_i c_i^0 \exp\left(-\frac{z_i e \psi(\vec{r})}{k_B T}\right) \right] = 0 \quad (3)$$

where $\psi(\vec{r})$ denotes electrostatic potential in the whole space, \vec{r} are positions in the Cartesian space, $\rho(\vec{r})$ is the density of fixed molecular charges, and the sum represents the mean concentration of z_i -valent ions given by the Boltzmann distribution where c_i^0 is the ion concentration in the bulk and e is the proton charge. In BD, a ligand moves in the potential generated by the rigid acceptor obtained from the numerical solution of the Poisson–Boltzmann equation on a three-dimensional grid. Intermolecular forces are computed considering the ligand as a set of point charges immersed in continuum solvent.⁴²

Electrostatic Potential Grids. The electrostatic potential (at ionic strengths equivalent to NaCl concentrations of 100, 150, 200, 300, 350, 400, 450, and 500 mM and temperature of 293 K) was calculated by solving the nonlinear Poisson–Boltzmann equation (eq 3) with the APBS package.⁴³ Three dimensional cubic grids of $353 \text{ \AA} \times 353 \text{ \AA} \times 353 \text{ \AA}$ and 1.05 \AA spacings in each direction centered on the 30S subunit were used. The multiple Debye–Hückel boundary conditions and focusing were applied.⁴³ The ϵ of the 30S subunit was set to 4 and that of the solvent to 78.54. The Richards accessible surface⁴⁴ with the probe radius of 1.4 \AA defined the dielectric boundary. The Stern ion exclusion layer was set to 2 \AA .

BD Simulations. University of Houston Brownian Dynamics package⁴⁰ was used to solve the equations of Brownian motion. For each ionic strength an ensemble of 50000 trajectories was generated. All trajectories began with the initial antibiotic–30S subunit separation of 300 \AA (b radius in Figure 3) and were truncated when the center-to-center distance of the acceptor and the ligand was above 600 \AA (q radius in Figure 3). A variable Δt was used: 0.1 ps in the region $\leq 170 \text{ \AA}$ around 30S subunit, 0.5 ps between 170 and 250 \AA , 1.0 ps between 250 and 325 \AA and 1.5 ps above 325 \AA . To account for the steric exclusion by the acceptor and for acceptor flexibility, antibiotic beads were assigned exclusion radii of 2 \AA . This value defines van-der-Waals-like contacts between paromomycin beads and 30S subunit atoms. Encounter complex formation was assessed by the distance of paromomycin's central bead and the backbone P atom of G1405 located in the A-site (Figure 2). We assumed a reaction when this distance was less than 10 \AA ($\sim 8.5 \text{ \AA}$ in the crystal structure). A single distance to define the reaction was used because with the coarse-grained antibiotic model

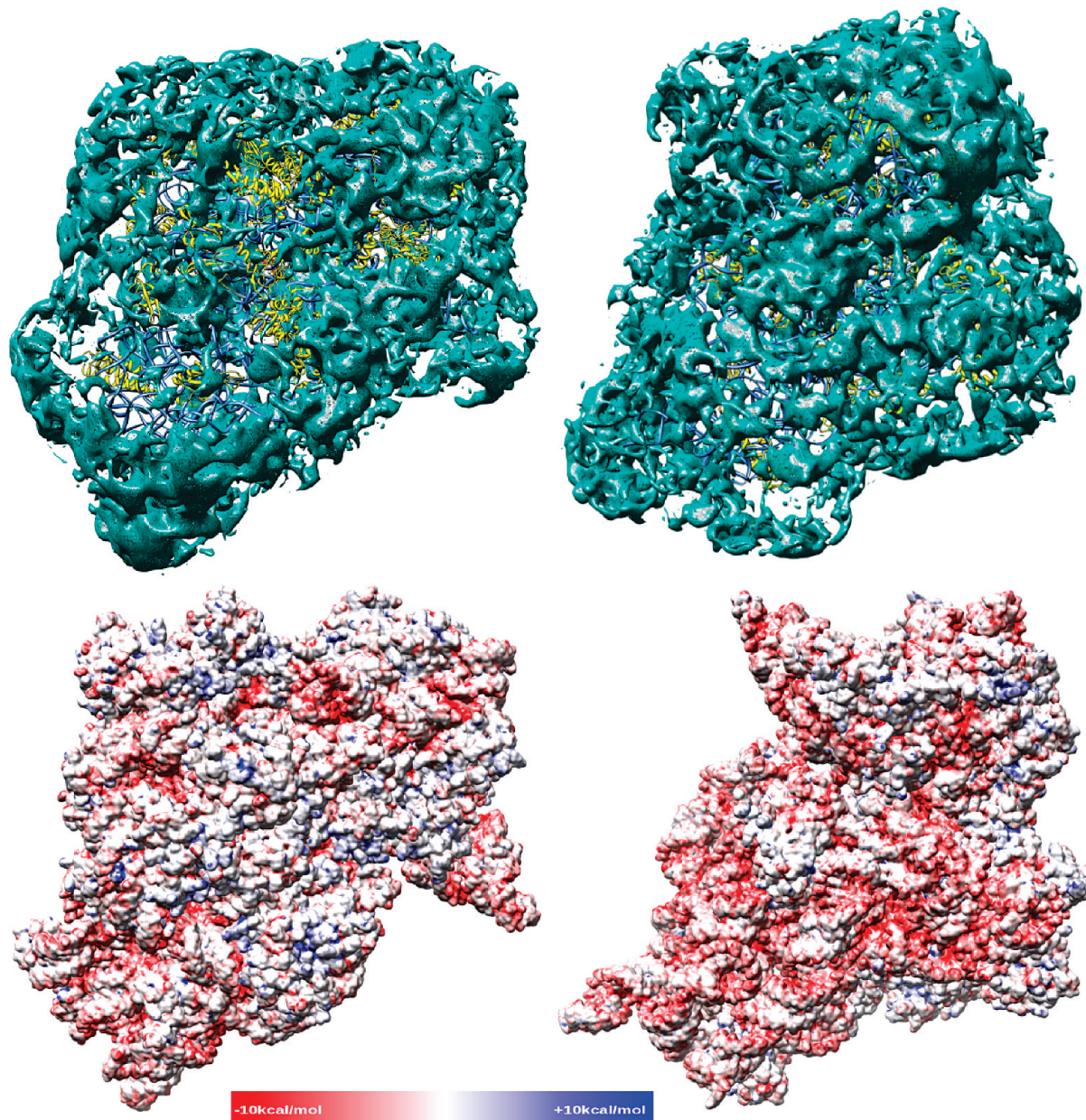


Figure 4. (Top) Isosurface of the ligand density (cyan mesh) computed on the basis of BD trajectories at 150 mM ionic strength. (Bottom) The electrostatic potential at 150 mM ionic strength projected onto the van der Waals surface of the 30S subunit. (Left) Solvent exposed side of the 30S subunit. (Right) 50S-interface side of the 30S subunit.

detailed information about its orientation inside the binding site is lost; somewhat “loose” definition applied here is consistent with the fact that the encounter complex describes a state located near the transition state on the path leading to the reaction instead of a tight, bound complex observed in the crystal structure.⁴⁵

Density Maps. Density maps representing positions of paromomycin around the acceptor were constructed based on 50000 BD trajectories generated at 150 mM ionic strength. The recorded ligand geometric center positions were transcribed into points belonging to a regular cubic grid, with dimensions of 193 Å × 193 Å × 193 Å and a 1.5 Å spacing, enclosing the acceptor; that is, a three-dimensional histogram was constructed. For both 30S variants the same grid center and orientation were used. Density maps were smoothed by convolution with a Gaussian function. Visualizations of maps and molecular structures as well as analysis were performed with UCSF Chimera.⁴⁶

Results

Association Pathways. Most proteins building the 30S ribosomal subunit are located at its external, solvent exposed side. The opposite 50S-exposed side, which forms the interface between the subunits, is rather bare of proteins. This fact has important consequences for the electrostatic properties in proximity to the 30S subunit surface shown in Figure 4. Negatively charged 16S RNA backbone phosphate groups located at the intersubunit interface are a source of negative electrostatic potential while the exterior proteins show less negative or positive potential values. Figure 4 also shows the constant density surface of paromomycin computed from BD trajectories. Its location is in agreement with electrostatic properties of the 30S subunit. Positively charged paromomycin avoids close contacts with proteins that are all positively charged. The antibiotic exploring the interface between ribosomal subunits is also shown in Figure 5 with residues colored

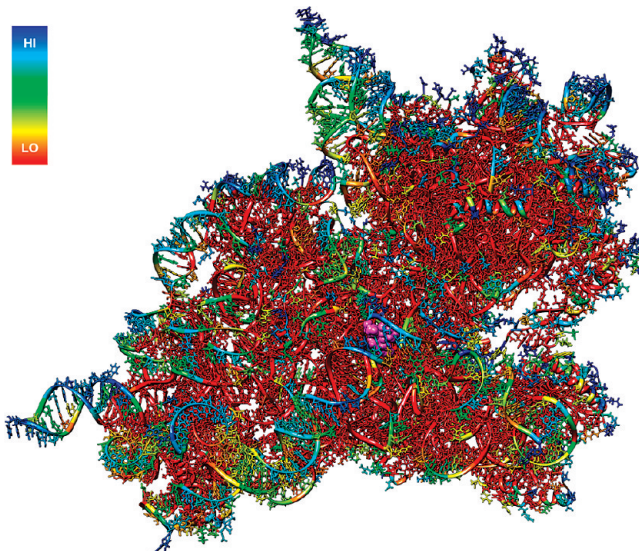


Figure 5. The atomic structure of the 50S-exposed side of the 30S subunit with residues colored according to ligand density derived from BD simulations at 150 mM ionic strength. Paromomycin bound at the A-site is shown in magenta.

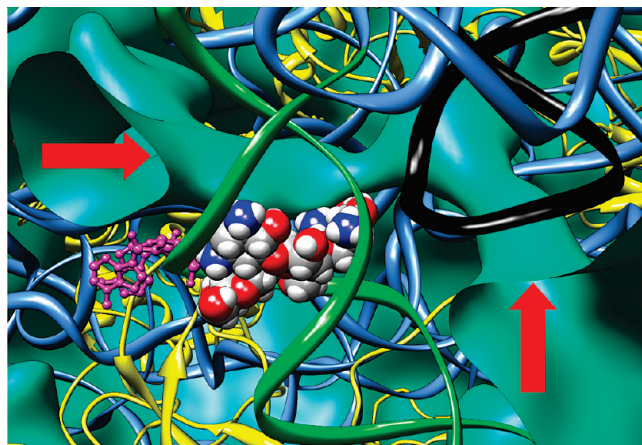


Figure 6. Isosurface of paromomycin density (cyan) in the vicinity of the ribosomal A-site. The antibiotic shown as van der Waals spheres is colored according to atom types. A1492 and A1493 are shown in magenta, helix 44 in green, and helix 45 in black. Red arrows indicate the entrances to the A-site.

according to the density of paromomycin. Significant paromomycin density is observed around RNA fragments located at the subunit's surface and along helix 44 (different regions of the 30S subunit are labeled in Figure 1).

Using density maps, we traced the paths taken by paromomycin to the A-site. First, the antibiotic diffuses toward the 30S subunit and next actively explores the subunit's surface “looking for” its specific binding site (an animation based on BD trajectories illustrating the described mechanism of association is presented in Supporting Information). There is no direct electrostatic steering toward the binding site. The 16S RNA negative phosphate group charges, distributed on the surface at the interface between the 30S and 50S subunits, distract the small antibiotic on its way toward the A-site (Figure 5). When the antibiotic finds itself in proximity of the A-site it can access it via two entrances. The constant density surface around the A-site displayed in Figure 6 shows that the antibiotic can access the binding site using either the entrance located between helices

45 and 44 or directly, from the other side of helix 44 using a funnel formed between the head and the shoulder of the 30S subunit.

Removing four tertiary proteins does not change the overall association mechanism. Figure 7 shows a differential density map constructed by subtracting the antibiotic density map obtained for the 30S subunit lacking S2, S3, S10, and S14 proteins, from that obtained for the whole 30S subunit. The only effect of the 30S particle modification on paromomycin association is that now the antibiotic targets the regions of the 30S subunit previously sterically blocked by these four proteins. The removal of four late binding proteins uncovers some RNA fragments from the 50S-exposed side and makes them accessible for paromomycin by creating a new attractive negatively charged area originating from the RNA phosphate groups. The presence of an antibiotic in this uncovered region may preclude binding of tertiary proteins causing the accumulation of the assembly intermediates.⁸ One needs to emphasize that removing the late binding proteins does not affect the accessibility of the A-site RNA to paromomycin.

Mobility of Paromomycin Near the A-Site. According to the results presented in Figure 6 the mobility of paromomycin in the vicinity of its binding site, that is, in the niche formed between the head and the shoulder of the 30S subunit, is high. The total volume of the continuous area located between the two entrances to the A-site and enclosed by the density isosurface depicted in Figure 6 (rear ends of arrows) is approximately $19.25 \times 10^3 \text{ \AA}^3$. The volume of the paromomycin bead model is 134 \AA^3 . The ratio of these two numbers gives a rough estimate of the antibiotic's mobility around its binding site (paromomycin can access a volume ~ 150 times larger than itself). An increased mobility of paromomycin is partially a consequence of a simplified coarse-grained antibiotic model and the lack of short-range interactions between paromomycin and RNA that are responsible for its preferential binding and positioning in the A-site. However, this fact influences only the simulation time scales and not the overall conclusions of this work. A sample movie presenting the behavior of paromomycin near the A-site prior to satisfying the reaction criteria is supplied as Supporting Information.

It was recently found by means of all-atom replica exchange molecular dynamics simulations⁴⁸ that gentamicin, another aminoglycosidic antibiotic, is also quite mobile in the A-site exploring a wide range of configurations. The antibiotic partially dissociates from the A-site and re-enters with motions of its center-of-mass on a 10 Å scale. This study confirms our results obtained from BD simulations of high mobility of antibiotic in the binding cleft, as well as the possibility of its shifting around in the binding site.

We also compared the regions visited by paromomycin with locations known to be the binding sites for other drugs targeting the 30S subunit: tetracycline,¹⁹ edeine,¹⁹ streptomycin,² spectinomycin,² pactamycin¹⁸ and hygromycin B¹⁸ (see Figure 8). Those structurally and electrostatically diverse ligands have different origins and modes of action.⁴⁷ However, as shown in Figure 8, the regions visited by paromomycin correlate with binding sites of other antibiotics. This suggests that the overall association mechanism is similar for all the considered drugs—they explore the surface of the acceptor in the absence of significant electrostatic steering toward the binding site, until they find a site where specific interactions (such as hydrogen bonds) stabilize their positions.

Interactions with Helix 44 of 16S RNA. Figure 1 presents some of the intersubunit bridges located at the interface between

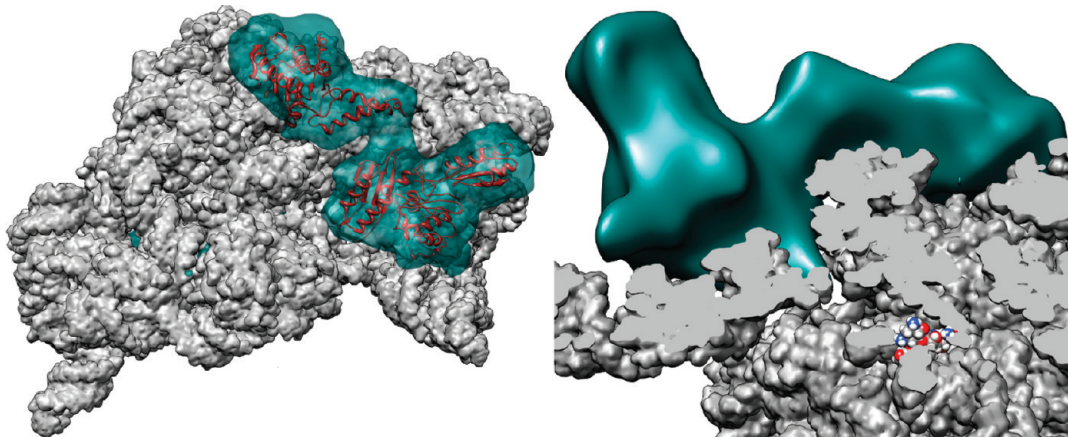


Figure 7. Left: Isosurface of the differential density map (partially transparent cyan) constructed from BD trajectories by subtracting the density maps of paromomycin diffusing in the electric field of the whole 30S subunit and of the 30S subunit without proteins S2, S3, S10, S14. Solvent-exposed side of the 30S particle is shown, with late binding proteins in red, and the remaining part of the 30S subunit as gray van der Waals surface. Right: View at the A-site from the 50S-exposed side showing that the removal of late binding proteins does not make the A-site more accessible to paromomycin (van der Waals spheres). The surface of the 30S subunit without proteins S2, S3, S10, S14 sliced perpendicularly to helix 44 is shown in gray and isosurface of the differential density map in cyan.

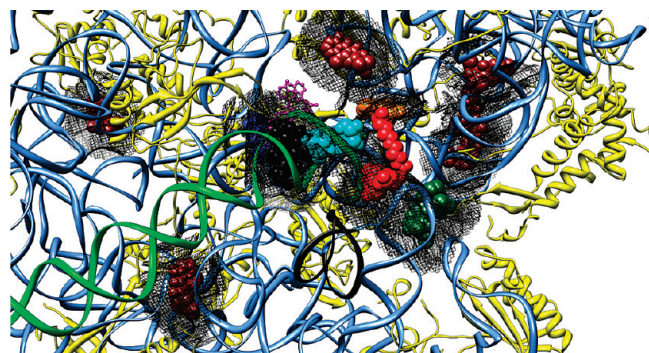


Figure 8. Binding sites of various antibiotics in the 30S *Thermus thermophilus* ribosomal subunit determined by X-ray crystallography. Paromomycin (black, PDB entries 1IBK and 1FJG), edeine (light red, PDB 1I95), hygromycin B (cyan, PDB 1HNZ), pactamycin (dark green, PDB 1HNX), spectinomycin (orange, PDB 1FJG), streptomycin (blue, PDB 1FJG), tetracyclines (dark red, PDB 1I97). Fragments of density isosurfaces from BD trajectories of paromomycin are shown as black mesh.

the 30S and 50S subunits and responsible for the formation of the 70S complex. Four bridges are formed by helix 44, namely B2a, B3, B5, and B6.⁴⁹ Recent experimental study¹³ suggested that paromomycin acts as an agent associating the ribosomal subunits most probably by stabilizing one or more intersubunit bridges which involve helix 44. Such association activity of paromomycin results from strengthening the interactions between ribosomal subunits and was found to be much stronger than a similar activity of Mg²⁺ ions.¹³ These positively charged agents screen the repulsive interactions between the negatively charged subunits in solution and decrease the density of negative charges at their interface. Such stabilization of 70S ribosomes by paromomycin may be in part responsible for its other inhibitory effect on translocation of tRNAs because paromomycin binding in the vicinity of intersubunit bridges may impede the relative ratchet-like movement of the subunits in the 70S complex. Such movement is required for tRNAs to translocate to their new positions on the ribosome after delivery of amino acids and formation of a peptide bond. Also, ribosome recycling may be affected due to overstabilization of the 70S complex which must dissociate into 30S and 50S subunits after termination of protein synthesis. However, a detailed mechanism of paromomycin subunit association activity is still unknown.¹³

Our studies indicate that regions favored by paromomycin are located also along helix 44 of 16S RNA (Figure 5). The movement of paromomycin in proximity to helix 44 is illustrated in Supporting Information. BD simulations reveal clefts close to helix 44 that are accessible to the antibiotic. For example, one such region is presented in Figure 8 and covers the area where the tetracycline binds, and two other regions are presented in Figure 9. The sliced density map shown in Figure 9 reveals a region characterized by significant density of paromomycin located near the bottom part of helix 44. The entrance to this alternate binding site is located in the vicinity of intersubunit bridges B6 and B8 (see Figure 1 and Figure 5) which suggests that high antibiotic density in this region may be important for its inhibitory role on the translocation of tRNAs. Perhaps aminoglycoside binding in this region restricts the relative movement of ribosomal subunits resulting in inhibition of translocation.¹³

To further check the presented hypothesis and describe the antibiotic association activity, one should simulate complexation and relative movement of both ribosomal subunits in the presence and absence of paromomycin. To the best of our knowledge, such a task is currently impossible due to limited capabilities of available BD packages and electrostatics methodology.

Association Rates. On the basis of BD simulations conducted at different ionic strengths we calculated paromomycin association rates that are shown in Figure 10. The rates were averaged over 5 sets of 10000 BD trajectories generated at a considered ionic strength and errors were computed as standard deviations. For both studied variants of the 30S subunit, association rates are of the order of $10^9 \text{ (M}\cdot\text{s)}^{-1}$ and almost no dependence on the ionic strength of the solution is observed. We find that the absence of ribosomal proteins S2, S3, S10, and S14 does not influence the antibiotic association rates.

To investigate the origins of the observed lack of the ionic strength dependence, we performed additional BD simulations; we excluded electrostatic interactions by neutralizing the antibiotic and setting all its bead charges to 0e. The computed association rate constant with electrostatics “switched-off” (Figure 10) is of the same magnitude as the rates obtained for a charged paromomycin signifying that the influence of electrostatic interactions on association rates is surprisingly weak.

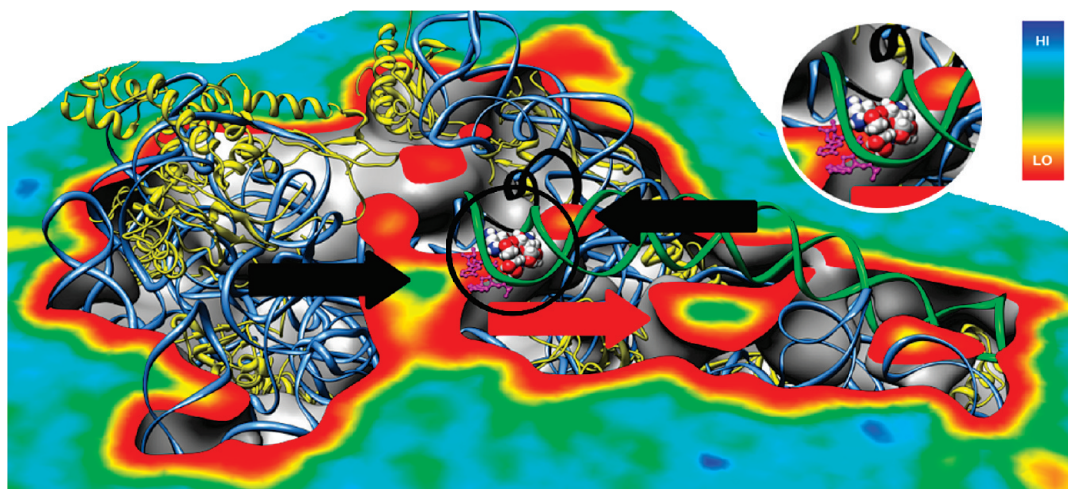


Figure 9. Density map sliced parallelly to the axis of helix 44 (in green). Paromomycin bound at the A-site is shown as van der Waals spheres (inside the black circle; see also inset in the upper right corner). Helix 45 is shown in black. Black arrows denote the two entrances to the A-site. Red arrow points toward the alternative binding site. Density values observed at both entrances to the A-site and at the entrance to the alternate binding site are comparable (see color legend).

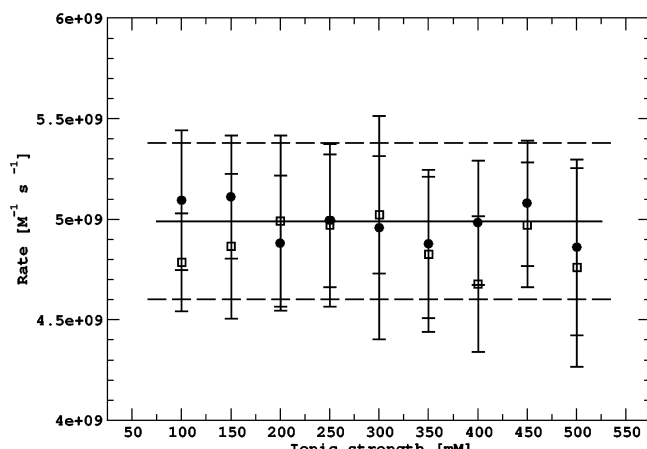


Figure 10. Ligand association rates computed from BD simulations at different ionic strengths of the solution. Black continuous and dashed horizontal lines show, respectively, the rates and errors calculated when the electrostatic interactions were switched off. Black circles and squares correspond to association rate constants obtained, respectively, for the ligand diffusing to the entire 30S subunit and the 30S subunit without proteins S2, S3, S10, S14.

To further verify this result, we performed BD simulations of a centrally $+5e$ charged sphere of a 5 Å radius diffusing in the electrostatic field generated by a spherical acceptor of a 100 Å radius and a central charge of $-1000e$ at ionic strengths ranging from 50 to 1000 mM. For such a model system also no ionic strength dependence of the association rates was observed. Additionally, we found that the association rate computed for a model neutral sphere is similar to the rates computed for the $+5e$ charged sphere.

The lack of the ionic strength dependence and the fact that electrostatic interactions do not influence the association rates are interesting physical results that can be explained as follows. In the studied range of ionic strength, the Debye length, that is, the effective range of electrostatic interactions, changes from 9.5 Å (in 100 mM) to 4.3 Å (in 500 mM). These distances are much smaller than the size of the 30S subunit whose overall dimensions are 215 Å \times 180 Å \times 202 Å but are on the order of antibiotic dimensions, 9 Å \times 14 Å \times 14 Å. At the lowest applied by us ionic strength of 100 mM, the electrostatic potential within the Debye length from the 30S subunit ranges

from -0.9 kcal/mol (-40 mV) to 0.3 kcal/mol (13 mV). At a distance of two Debye lengths (i.e., ~ 19 Å at 100 mM), the electrostatic potential almost vanishes varying from -0.3 kcal/mol (-13 mV) to 0.05 kcal/mol (2.2 mV). Therefore, there is no electrostatic interaction between the two diffusing molecules when they are far apart; in the BD simulations the initial separation of the antibiotic and the 30S subunit, that is, the b radius, is 300 Å. Paromomycin begins to “feel” the 30S particle only when the distance between the molecules is much smaller than the size of the acceptor. Moreover, at short distances paromomycin “sees” the acceptor almost as a planar surface. The limited range (as compared to the size of the acceptor) of electrostatic interactions makes the ligand target various regions of the 30S subunit surface with almost equal and independent of ionic strength probabilities. The investigation of electrostatic potentials presented in Figure 4 and described above reveals a number of negative electrostatic potential patches that distract paromomycin on its way to the A-site. The antibiotic diffuses between such negative spots, interacting with the nearby 30S subunit charges (within the range defined by the Debye length), and eventually finds its specific binding site.

The same mechanism applies also to the association of paromomycin toward the variant of the 30S particle lacking four late binding proteins S2, S3, S10, and S14. The fact that the absence of these proteins does not influence the antibiotic association rates can be explained as follows. After removing of tertiary proteins the total surface area of the 30S particle decreases by approximately 7%. This constitutes only a small change of the total surface that can be targeted by the ligand. Additionally, the removal of these proteins does not make the A-site more accessible to the ligand (see Figure 7). Without electrostatic steering toward the binding site the probability of finding a specific site (and in effect the association rate constant) depends mostly on the ratio of the site’s area to the area of the whole acceptor. This ratio remains almost unchanged upon removal of proteins S2, S3, S10, S14, therefore, we observe no change in the computed association rate constants.

Conclusions

Using Brownian dynamics methodology, we investigated the mechanism and kinetics of association of an aminoglycosidic antibiotic, paromomycin, with the 30S ribosomal subunit. The

considered 30S system is challenging due to its size, high density of negative charges located on the subunit's surface, and multitude of different RNA motifs explored by the ligand upon binding.

We found that there is no direct electrostatic steering of the antibiotic toward the specific binding site. Paromomycin association mechanism relies on inspecting the surface of the subunit prior to finding the A-site binding cleft. We observed that the antibiotic can access the A-site via two entrances located on the opposite sides and its mobility in the binding site is quite high. The aminoglycoside can also search alternative cavities that are the binding sites for other known antibiotics.

We estimated the antibiotic association rates of about 10^9 $(M \cdot s)^{-1}$ with no dependence on the ionic strength in the range of 100–500 mM. Contrary to results obtained for a number of protein complexes, including thrombin and hirudin,⁵⁰ barnase and barstar,^{27,28} ferricytochrome c and ferrocyanochrome b₅,⁵¹ where protein–protein association is enhanced by interaction potentials,⁵² the role of electrostatics during association is limited due to the enormous size of the 30S particle when compared to the effective range of electrostatic interactions in ionic solutions. However, we were not able to verify these results due to lack of experimental data and it is hard or almost impossible to find a comparable system as a reference.

We described local interactions of paromomycin with regions of 16S RNA helix 44 forming intersubunit bridges. We observed that paromomycin targets the clefts located near the intersubunit bridges B6 and B8. All these interactions might be responsible for overstabilization of the 70S complex, another recently suggested paromomycin's inhibitory effect.¹³ Alternative binding clefts revealed by BD simulations are accessible to paromomycin and the negative electrostatic potential observed in their vicinity may promote binding of the antibiotic at those sites. One should, nevertheless, keep in mind that with such a simplified ligand model and the lack of short-range interactions, we were not able to describe in detail the orientation of paromomycin and its close intermolecular contacts. Therefore, we can neither confirm whether the binding of paromomycin at a particular site can be specific nor quantitatively estimate the affinity of such binding. Answering this question would require a different kind of study that employs an atomistic model of the ligand with a detailed description of its interactions with the 30S particle and optimization or docking algorithms. However, with BD methodology we were able to show that alternative binding sites may exist on the 30S particle and that their locations correlate with experimental observations.

The BD methodology applied in this work is not free of limitations. The 30S subunit is represented with a single, rigid conformation and flexibility of the acceptor is taken into account only indirectly, by specifying appropriate exclusion radii of antibiotic beads. Additionally, the four-bead representation of paromomycin partially loses the information about antibiotic orientation near the surface of the 30S particle. These limitations should not influence the computed rate constants and the description of the overall association mechanism, that is, the absence of direct electrostatic steering toward the binding site and the lack of ionic strength dependence of association rate constants. Another BD limitation is related to the fact that only electrostatic interactions are considered when generating ligand trajectories and short-ranged and hydrodynamic forces are neglected. Evaluation of the latter terms during simulations would be too demanding from the computational standpoint. While the presence of short-ranged forces would not influence the overall long-range association process their role becomes

important at small intermolecular separations. van der Waals, hydrodynamic and solvation forces may oppose or act in concert with electrostatics, influencing ligand binding at specific acceptor's sites.⁵³

The kinetics of association of the 30S ribosomal subunit–antibiotic complex has not been studied previously neither experimentally nor computationally, and we could not compare our results with those obtained with another method. However, we have shown the details of the association that may become helpful for understanding the mechanisms of small antibiotic binding to much larger receptors and paromomycin's various inhibitory roles on translocation of tRNAs and ribosome recycling.

Acknowledgment. We acknowledge support from University of Warsaw (115/30/E-343/BST1345/ICM/2008 and G31-4), Polish Ministry of Science and Higher Education (3 T11F 005 30, 2006–2008), Fogarty International Center (NIH grant no. R03 TW07318) and Foundation for Polish Science. We would like to thank Jan Antosiewicz for helpful discussions and critical reading of the manuscript and J. Andrew McCammon and CTBP for supporting authors' visits at University of California at San Diego.

Supporting Information Available: Two movies of paromomycin associated with the 30S subunit and the A-site. This material is available free of charge via the Internet at <http://pubs.acs.org>.

References and Notes

- Kaul, M.; Barbieri, C. M.; Kerrigan, J. E.; Pilch, D. S. *J. Mol. Biol.* **2003**, *326*, 1373–1387.
- Carter, A. P.; Clemons, W. M. J.; Brodersen, D. E.; Morgan-Warren, R. J.; Wimberly, B. T.; Ramakrishnan, V. *Nature* **2000**, *407*, 340–348.
- Ogle, J. M.; Brodersen, D. E.; Clemons, W. M. J.; Tarry, M. J.; Carter, A. P.; Ramakrishnan, V. *Science* **2001**, *292*, 897–902.
- Moazed, D.; Noller, H. *Nature* **1987**, *327*, 389–394.
- Fourmy, D.; Recht, M. I.; Blanchard, S. C.; Puglisi, J. D. *Science* **1996**, *274*, 1367–1371.
- Ogle, J. M.; Carter, A. P.; Ramakrishnan, V. *Trends Biochem. Sci.* **2003**, *28*, 259–266.
- Mehta, R.; Champney, W. S. *Antimicrob. Agents Chemother.* **2002**, *46*, 1546–1549.
- Foster, C.; Champney, W. S. *Arch. Microbiol.* **2008**, *189*, 441–449.
- Nierhaus, K.; Bordash, K.; Homann, H. E. *J. Mol. Biol.* **1973**, *74*, 587–597.
- Powers, T.; Daubresse, G.; Noller, H. F. *J. Mol. Biol.* **1993**, *232*, 362–374.
- Culver, G. M. *Biopolymers* **2003**, *68*, 234–249.
- Mizushima, S.; Nomura, M. *Nature* **1970**, *226*, 1214–1218.
- Hirokawa, G.; Hideko, K.; Kaji, A. *Antimicrob. Agents Chemother.* **2007**, *51*, 175–180.
- Vicens, Q.; Westhof, E. *Structure* **2001**, *9*, 647–658.
- Han, Q.; Zhao, Q.; Fish, S.; Simonsen, K. B.; Vourloumis, D.; Froelich, J. M.; Wall, D.; Hermann, T. *Angew. Chem., Int. Ed.* **2005**, *44*, 2694–2700.
- Vicens, Q.; Westhof, E. *J. Mol. Biol.* **2003**, *326*, 1175–1188.
- Vicens, Q.; Westhof, E. *Chem. Biol.* **2002**, *9*, 747–755.
- Brodersen, D. E.; Clemons, W. M. J.; Carter, A. P.; Morgan-Warren, R. J.; Wimberly, B. T.; Ramakrishnan, V. *Cell* **2000**, *103*, 1143–1154.
- Pioletti, M.; Schlunzen, F.; Harms, J.; Zarivach, R.; Gluhmann, M.; Avila, H.; Bashan, A.; Bartels, H.; Auerbach, T.; Jacobi, C.; Hartsch, T.; Yonath, A.; Franceschi, F. *EMBO J.* **2001**, *20*, 1829–1839.
- Hermann, T.; Westhof, E. *J. Med. Chem.* **1999**, *42*, 1250–1261.
- Murray, J. B.; Meroueh, S. O.; Russell, R. J. M.; Lentzen, G.; Haddad, J.; Mabashery, S. *Chem. Biol.* **2006**, *13*, 129–138.
- Vaiana, A. C.; Westhof, E.; Auffinger, P. *Biochimie* **2006**, *88*, 1061–1073.
- Sanbonmatsu, K. Y. *Biochimie* **2006**, *88*, 1053–1059.
- Dlugosz, M.; Antosiewicz, J. M.; Trylska, J. *J. Chem. Theory Comput.* **2008**, *4*, 549–559.
- Ma, C.; Baker, N. A.; Joseph, S.; McCammon, J. A. *J. Am. Chem. Soc.* **2002**, *124*, 1438–1442.

- (26) Yang, G.; Trylska, J.; Tor, Y.; McCammon, J. A. *J. Med. Chem.* **2006**, *49*, 5478–5490.
- (27) Gabdoulline, R. R.; Wade, R. C. *Biophys. J.* **1997**, *72*, 1917–1929.
- (28) Spaar, A.; Dammer, C.; Gabdoulline, R. R.; Wade, R. C. *Biophys. J.* **2006**, *90*, 1913–1924.
- (29) Tan, R. C.; Truong, T. T.; McCammon, J. A.; Sussman, J. L. *Biochemistry* **1993**, *32*, 401–403.
- (30) Das, A.; Jayaram, B. *J. Mol. Liq.* **1998**, *77*, 157–163.
- (31) Berman, H. M.; Westbrook, J.; Feng, Z.; Gilliland, G.; Bhat, T. N.; Weissig, H.; Shindyalov, I. N.; Bourne, P. E. *Nucleic Acids Res.* **2000**, *28*, 235–242.
- (32) Pearlman, D. A.; Case, D. A.; Caldwell, J. W.; Ross, W. S.; T. E. Cheatham, I.; DeBolt, S.; Ferguson, D.; Seibel, G.; Kollman, P. *Comput. Phys. Commun.* **1995**, *91*, 1–41.
- (33) Cui, Q.; Tan, R. K.-Z.; Harvey, S. C.; Case, D. A. *Multiscale Model. Simul.* **2006**, *5*, 1248–1263.
- (34) Wang, J.; Wang, W.; Kollman, P. A.; Case, D. A. *J. Mol. Graphics Modell.* **2006**, *24*, 247–260.
- (35) Ermak, D. L.; McCammon, J. A. *J. Chem. Phys.* **1978**, *69*, 1352–1360.
- (36) Northrup, S. H.; Hynes, J. T. *J. Chem. Phys.* **1979**, *71*, 871–883.
- (37) Northrup, S. H.; Allison, S. A.; McCammon, J. A. *J. Chem. Phys.* **1984**, *80*, 1517–1524.
- (38) de la Torre, G. *Biophys. Chem.* **2001**, *94*, 265–274.
- (39) Antosiewicz, J. *Biophys. J.* **1995**, *69*, 1344–1354.
- (40) Madura, J. D.; Briggs, J. M.; Wade, R. C.; Davis, M. E.; Luty, B. A.; Ilin, A.; Antosiewicz, J.; Gilson, M. K.; Bagheri, B.; Scott, R. L.; McCammon, J. A. *Comput. Phys. Commun.* **1995**, *91*, 57–95.
- (41) Gilson, M. K.; Honig, B. H. *Proteins: Struct., Funct., Genet.* **1988**, *3* (1), 32–52.
- (42) Davis, M. E.; Madura, J. D.; Luty, B. A.; McCammon, J. A. *Comput. Phys. Commun.* **1991**, *62*, 187–197.
- (43) Baker, N. A.; Sept, D.; Joseph, S.; Holst, M. J.; McCammon, J. A. *Proc. Natl. Acad. Sci. U.S.A.* **2001**, *98*, 10037–10041.
- (44) Richards, F. M. *Annu. Rev. Biophys. Bioeng.* **1977**, *6*, 151–176.
- (45) Spaar, A.; Helms, V. *J. Chem. Theory Comput.* **2005**, *1*, 723–736.
- (46) Pettersen, E. F.; Goddard, T. D.; Huang, C. C.; Couch, G. S.; Greenblatt, D. M.; Meng, E. C.; Ferrin, T. E. *J. Comput. Chem.* **2004**, *25*, 1605–1612.
- (47) Liljas, A. *Structural Aspects of Protein Synthesis*; World Scientific Publishing Co.: River Edge, NJ, 2004.
- (48) Vaiana, A. C.; Sanbonmatsu, K. Y. *J. Mol. Biol.* **2009**, *386*, 648–661.
- (49) Yusupov, M. M.; Yusupova, G. Z.; Baucom, A.; Lieberman, K.; Earnest, T. N.; Cate, J. H. D.; Noller, H. F. *Science* **2001**, *292*, 883–896.
- (50) Stones, R. S.; Denis, S.; Hofsteenge, J. *Biochemistry* **1989**, *28*, 6857–6863.
- (51) Eltis, L. D.; Herbert, R. G.; Baker, P. D.; Mauk, A. G.; Northrup, S. H. *Biochemistry* **1991**, *20*, 3663–3674.
- (52) Zhou, H. X. *Biophys. J.* **1997**, *73*, 2441–2445.
- (53) Leckband, D.; Sivasankar, S. *Colloids Surf. B: Biointerfaces* **1999**, *14*, 83–97.

JP8112914